VSP

*Advanced Robotics 22 (2008) 829–849*

ADVANCED ROBOTICS
www.brill.nl/ar

*Full paper*

# Biomimetic Tactile Sensor Array

**Nicholas Wettels** [a,*], **Veronica J. Santos** [a], **Roland S. Johansson** [b] **and Gerald E. Loeb** [a]

[a] A. E. Mann Institute and Biomedical Engineering Department, University of Southern California, 1042 Downey Way DRB-101, Los Angeles, CA 90089, USA

[b] Physiology Section, Department of Integrative Medical Biology, Umeå University, 901 87 Umeå, Sweden

Received 3 August 2007; accepted 28 September 2007

**Abstract**

The performance of robotic and prosthetic hands in unstructured environments is severely limited by their having little or no tactile information compared to the rich tactile feedback of the human hand. We are developing a novel, robust tactile sensor array that mimics the mechanical properties and distributed touch receptors of the human fingertip. It consists of a rigid core surrounded by a weakly conductive fluid contained within an elastomeric skin. The sensor uses the deformable properties of the finger pad as part of the transduction process. Multiple electrodes are mounted on the surface of the rigid core and connected to impedance-measuring circuitry safely embedded within the core. External forces deform the fluid path around the electrodes, resulting in a distributed pattern of impedance changes containing information about those forces and the objects that applied them. Here we describe means to optimize the dynamic range of individual electrode sensors by texturing the inner surface of the silicone skin. Forces ranging from 0.1 to 30 N produced impedances ranging from 5 to 1000 kΩ. Spatial resolution (below 2 mm) and frequency response (above 50 Hz) appeared to be limited only by the viscoelastic properties of the silicone elastomeric skin.



**Keywords**

Biomimetic, electrode impedance, pressure sensor, haptics, tactile sensor

## 1. Introduction

Currently, robotic manipulanda excel in structured environments built around the robot, as in the automotive industry. The performance of robotic and prosthetic hands in unstructured environments, however, is severely limited by their having little or no tactile information compared to the rich tactile feedback of the human hand. Advancements in sensor hardware will undoubtedly cascade into equally

* To whom correspondence should be addressed. E-mail: nick.wettels@gmail.com

 DOI:10.1163/156855308X314533

important advancements in controller design and grasp planning algorithms. Numerous fields of research would benefit from such advances: prosthetics [1], anthropomorphic robotics [2], tele-operated and autonomous robotics [3], robotic and telesurgery [4, 5], telediagnostics and palpation [6].

A wide variety of technologies have been applied to solve the tactile sensing problem in robotics and medicine [7]. Transduction mechanisms such as optics, capacitance, piezoresistance, ultrasound, conductive polymers, etc., have all yielded viable solutions, but only for limited environments or applications. For example, most MEMS sensors provide good resolution and sensitivity, but lack the robustness for many applications outside the laboratory [8–10]. Beebe proposed a piezoresitive silicon-based MEMS sensor with a high tensile strength, but the sensor was limited by hysteresis and the inability to sense shear forces [11], which are just as important for grip control as normal forces. Conductive particles [12] suspended in elastomers can result in elastic materials whose resistivity changes with deformation. A recent enhancement of such materials called quantum tunneling composites greatly increases sensitivity and dynamic range, but at the expense of mechanical hysteresis and simultaneous sensitivity to temperature and absorption of gases [12]. Hysteresis alone may preclude the development of real-time grip control algorithms with short latencies similar to those observed in humans.

The curved, deformable nature of biological fingertips provides mechanical features that are important for the manipulation of the wide variety of objects encountered naturally. Multi-axis force sensing arrays have been fabricated using MEMS, but they are not suitable for mounting on such surfaces or for use in environments that include heavy loads, dust, fluids, sharp edges and wide temperature swings [9, 10]. If protective, skin-like elastic coverings are placed on top of sensor arrays, they desensitize the sensors and function as low-pass temporal and spatial filters with respect to incident stimuli [13]. Therefore, we considered it beneficial to make the cosmesis (skin) part of the transduction process rather than fighting it after the fact. This led to the approach of using a fluid in an elastomer as the transduction mechanism. Recently, flexible sensors have been developed to allow the mounting of the sensor on curved surfaces [14, 15]. However, these sensors cannot detect shear forces and their delicate electronic components are vulnerable to damage when mounted directly on gripping surfaces.

Helsel *et al.* described an impedance-based sensor using a planar grid of gold–chromium electrodes, ethylene glycol-based conductive fluid and latex skin [16]. Another fluid-filled sensor measured the impedance between electrodes on the inner surface of the elastomeric skin and on the surface of the core [17, 18]. These sensors were designed to detect deflection of the skin, but would saturate or otherwise fail at forces that caused contact with the core. Fingertips that employ electrorheological fluids for dynamic shape control use plates to apply high voltage fields. These plates can be used for capacitive sensing, but practical arrays have encountered problems including arcing [19, 20].

Here we describe a biomimetic tactile sensor that is sensitive to the wide range of normal and shear forces encountered in robotic and prosthetic applications. It is intrinsically simple, robust, and easy to manufacture and repair. This report focuses on a novel approach to extending the dynamic range by texturing the inner surface of the elastomeric skin. Preliminary results indicate promising spatial and temporal resolution.

## 2. Methods

### *2.1. Design Concept*

Our tactile sensor, modeled after the human digit, consists of a rigid central core surrounded by a weakly conductive fluid contained within a silicone elastomeric 'skin' (Fig. 1) [21]. As with biological fingertips, our design incorporates the low-pass filter effects of cosmetic, protective skin and fluid into the transduction process. The skin is resistant to wear, and possesses texture and tackiness similar to the properties that facilitate grip by biological fingertips. Electrodes are distributed along the surface of the rigid core and all sensitive components are safely embedded within the core. By applying an alternating current to each contact, one can measure the impedance of each volumetric flow path from a given contact to a reference electrode. External forces deform the fluid path around the electrodes, resulting in a distributed pattern of impedance changes containing information about force magnitude, direction, point of contact and object shape.

### *2.2. Prototype Fabrication and Theory of Transduction*

Fabrication and results from an early prototype are described in a previous conference paper [22]. To create the rigid core of the array described here, we machined jeweler's wax to create a negative mold of a shape similar to the distal phalanx of a human finger, with its tapered body and flat gripping surface. Individual gold contacts were formed by melting the end of a 5-μm Parylene-C insulated, 0.25-mm diameter gold wire into a ball and swaging to a 2.3-mm diameter, 0.5-mm thick disk. The contacts were tacked to the inside of the negative mold and the wire leads were soldered to a multi-pin electrical connector. A capillary tube was affixed in the mold for later use to inflate the fingertip with fluid. The mold was filled with liquid dental acrylic (Hygenic; Perm reline/repair resin) and cured to form a rigid finger core with electrodes on its surface. The sensor has no moving parts, and delicate electrical components and wiring are protected in the high-strength rigid core (compressive strengths 10–100 MPa and tensile strength 1–10 MPa [23]).

The choice of silicone elastomer for the skin depends on achieving mechanical properties and cosmetic appearance similar to normal skin. Candidate outer materials include Dragon Skin (Smooth-On Inc.; Shore A hardness of 10 and tear strength of 102 lb/in) and VST-30 (Factor II Shore A hardness of 23 and tear strength of 100 lb/in). A higher durometer inner coating can be used to optimize mechanical properties, while a softer, outer coating will provide a cosmetic appearance and

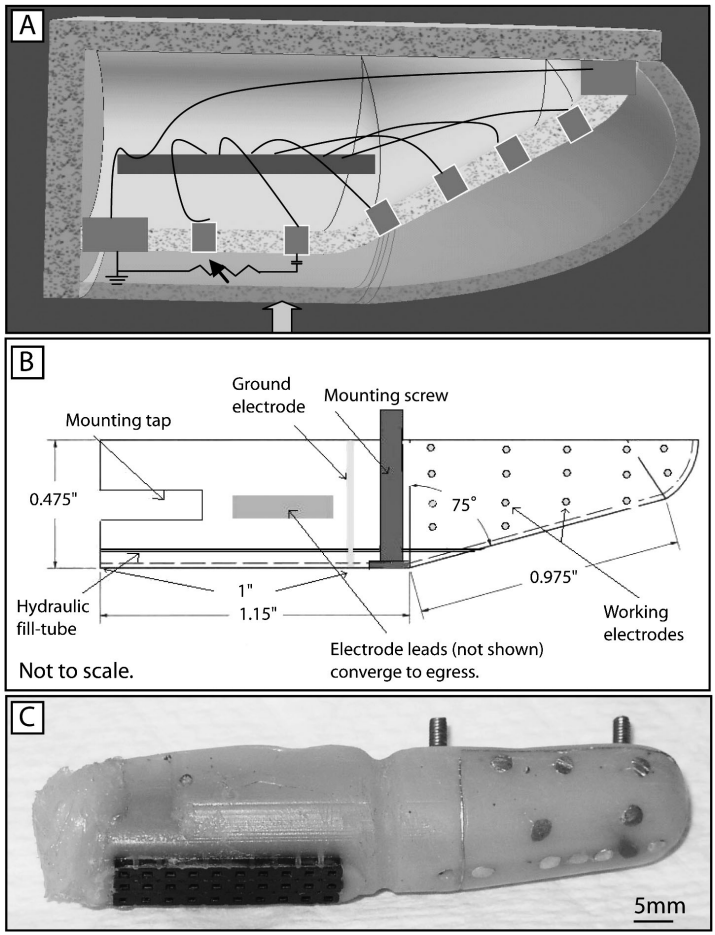


**Figure 1.** (A) Mechanical drawing of the biomimetic tactile sensor showing a rigid core shaped like the distal phalanx with an internal, sealed compartment for electronics connected to sensing electrodes in contact with a weakly conductive fluid under a viscoelastic skin. (B) Mechanical drawing of the current core design with a sample electrode layout. (C) Current acrylic prototype core with skin and fingernail removed. The thin gold ground electrode, circular gold working electrodes and blue thermistor are visible on the surface of the core.

feel. The coating of the elastomeric skin onto the rigid core enables easy repair of the most vulnerable part of any finger. The skin is easily replaced without any effects on the sensing electrodes or their supporting electronic circuitry within the rigid core. A plastic fingernail was used to anchor the skin to the core on the dorsal side of the fingertip. This feature contributes to the sensitivity of the sensing array to tangential as well as normal forces [22], but it is not studied in this report. Salt water (described later) was introduced through the fill-tube at the proximal end of the fingertip to inflate the cured silicone skin away from the core. In the future, mechanical fixation features can be incorporated into the mold to facilitate mounting of the fingertip to a mechatronic hand or mechanical test setup.

**Table 1.**
Effects of texturing of the internal surface of the skin on sensor behavior were studied for multiple combinations of silicone stiffness and sandpaper grit size

| Silicone durometer (Shore A hardness) | Sandpaper grit size | |
|---|---|---|
| | 60 (rough) | 100 (fine) |
| 10 (compliant) | | ✓ |
| 45 | | ✓ |
| 60 (stiff) | ✓ | ✓ |

Saturation of an electrode occurs when it becomes completely occluded, the volumetric flow path cannot become any more resistive and the impedance measurements do not increase. Texturing of the internal surface of the skin allows for small conductive pathways to exist even after the internal surface of the skin has been compressed against the electrode and increases the upper limit on the force-sensing range of the sensor. Thus, for preliminary characterization testing, we varied the stiffness and texture of the internal surface of the skin to investigate their effects on sensing behavior (Table 1). Strips of sandpaper of various grit sizes were used as the negative molds for test strips ($9 \times 20$ mm) of textured silicone. These strips served as the internal surface of the skin while a softer, untextured Dragon Skin silicone elastomer served as the outer surface.

The sensitivity of the device depends complexly on the conductivity of the fluid, the viscoelastic properties of the combined system of skin and pressurized fluid, volume and pressure of fluid, and the material and geometry of the electrode contacts. It is generally desirable for the fluid to have a low viscosity to minimize damping and hysteresis, and a high resistivity so that the measured impedance of the series circuit (electrodes plus fluid) is dominated by the fluid resistance rather than the capacitive reactance of the metal–electrolyte interfaces. In the tests described here, the fluid was water with a low concentration of NaCl (0.75 g/l; 1/12th the concentration of physiological saline).

### *2.3. Signal Conditioning*

It is desirable to energize the electrode system in such a way that the voltages developed across the metal–electrolyte interfaces are sufficiently low to avoid Faradaic current flow, which would corrode the metal contacts and cause electrolysis of the electrolytic fluid [24]. This can be accomplished by applying a small, alternating current and measuring the resulting voltage across the electrodes. The capacitance of one working electrode and ground electrode were found empirically to be 84.25 nF. This is consistent with capacitance per unit area values found in the literature [25, 26]. For a given electrode this capacitance has a reactance of 1.89 kΩ

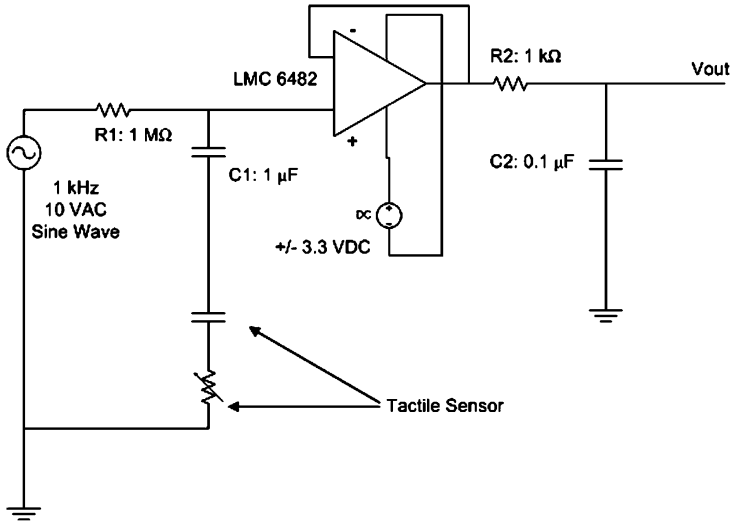


**Figure 2.** The signal-conditioning circuit used to collect characterization data from a single electrode.

at 1 kHz, which would be a small component of the dynamic range of the total impedance of the sensor (5–1000 kΩ).

The signal-conditioning circuit (Fig. 2) was driven with a 1-kHz 10-V AC sinewave in series with $R_1$ to provide a constant current source. Based on the dynamic range of sensor impedances to be measured, a 1-MΩ resistor was chosen for $R_1$. The voltage across the electrodes was buffered by a unity gain operational amplifier (National Semiconductor; LMC 6482) and frequencies higher than the 1-kHz test signal were filtered by $R_2C_2$. Capacitor $C_1$ blocked any DC bias from the sensor electrodes to prevent corrosion and electrolysis. $V_{out}$ was digitized at 50 kilosamples/s (National Instruments; SCB100). The double-layer capacitance between the electrolyte solution and the metal of the working electrode and ground electrode and fluid has been represented as a single capacitor in series with the variable resistor representing the deformable, volume-conductive fluid path between them. Peak-to-peak voltage was determined by a custom LabVIEW (National Instruments) program that translated this output into a calibrated impedance value for the graphs plotted herein.

### *2.4. Static Characterization of a Single Electrode*

To characterize the static behavior of a single electrode for the prototype shown in Fig. 1C, we applied normal forces to the electrode of interest and the surrounding area. A linear drive (Nippon Pulse America; PFL35T-48Q4C(120) stepper motor and NPAD10BF chopper drive) was used to advance interchangeable probes: 2 mm diameter (1 mm radius of curvature) and 20 mm diameter (11 mm radius of curvature), and a large flat plate (2.6 × 3.3 cm). The probes were designed to have radii of curvature much smaller than, approximately equal to and much larger than the curvature of the sensor core, respectively. Deflection was recorded from the point

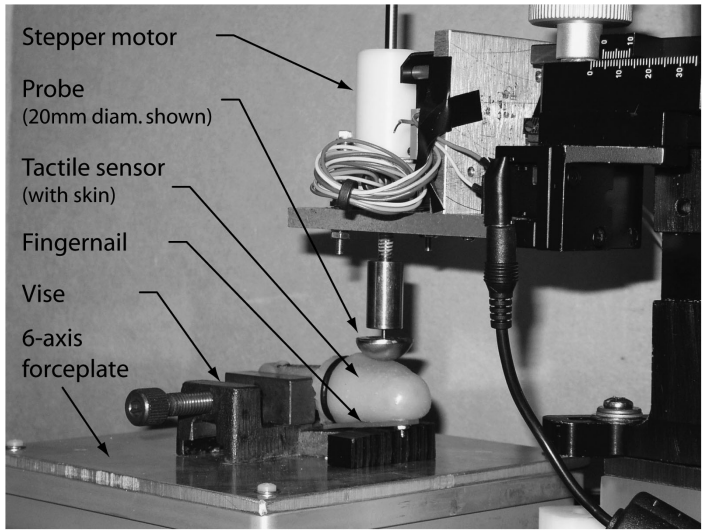


**Figure 3.** Experimental set-up for static characterization of a single electrode.

of the initial probe contact with the skin. Normal force was measured using a six-axis forceplate (Advanced Mechanical Technology; HE6X6-16) positioned below the vise holding the sensor (Fig. 3).

To characterize the spatial resolution of an electrode, the sensor was systematically probed in a $4 \times 5$ grid in 2 mm increments centered on the electrode. All impedance measurements were obtained at 4.5 mm indentation.

## 3. Results

### *3.1. Static Characterization of a Single Electrode*

#### *3.1.1. Deflection Applied Directly Above the Electrode*

As the fingertip was compressed, there was a monotonic but nonlinear increase in electrode impedance over a range of 100–1000 times the starting value (Fig. 4). The slopes of the curves depended complexly on probe curvature, as discussed later. The reaction force of the fingertip also rose monotonically and nonlinearly as the fluid was displaced from under the skin (region A in Fig. 4) and the skin was compressed against the rigid core (regions B and C). Region C is broken down into two areas: C(1) is the region where the textured surface contacts the core; C(2) is where sensor begins to saturate, as maximal occlusion of the electrode occurs. The sigmoidal shape of these logarithmic curves is reminiscent of many biological transducers, which generally need to optimize local sensitivity over a wide dynamic range of possible inputs [28].

Figure 5A–C shows how the sensor responded to variations in texture when indented with the 20-mm probe. For Fig. 5A, in the case of no texturing (10 durometer, no texture curve) the impedance rose very quickly to infinity once forces

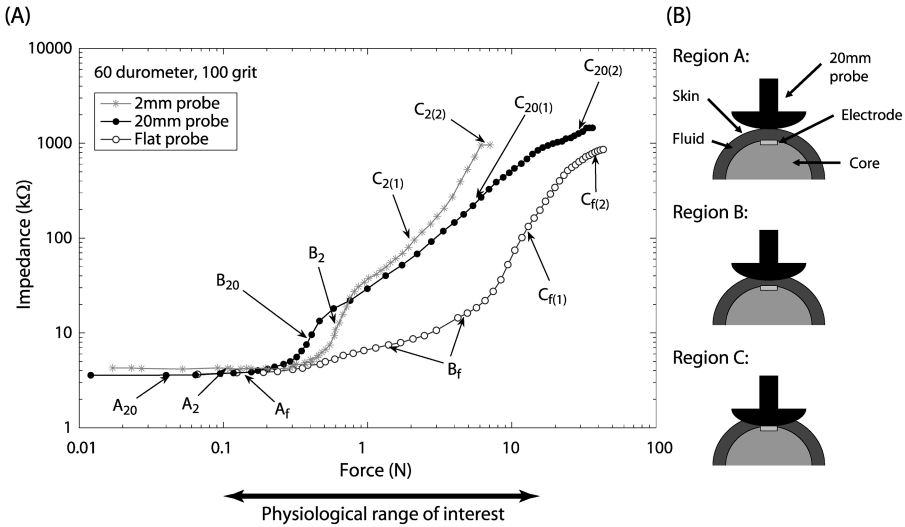


**Figure 4.** (A) Impedance (log scale) as a function of force (log scale) applied normal to the electrode surface. Textured silicone: 60 durometer, 100 grit size. (B) Graphic correlating curve shapes to probe indentation (20-mm probe shown).

exceeded 1 N. To increase this dynamic range and decrease the impedance/force slope, internal texturing of the device was necessary. The stiffer the silicone texture used, the higher the forces required to maximally occlude a given electrode. Another factor affecting the contact point and the beginning of region C was the thickness of the textured strips. The 60 durometer strip contacted first and the 10 durometer last. Their thicknesses were 2, 1.6 and 1.2 mm for the 60, 45 and 10 durometer strips, respectively.

Figure 5B shows the effect of texture depth on the operating range of the sensor. The deeper the texture (grit size), the more force was required to occlude the electrode. Figure 5C illustrates the effect of sensor volume (and subsequently hydrostatic pressure) on the force–impedance curves. When the sensor was drained to 1 ml, the resting impedance increased because the finger was deflated, bringing the skin closer to the surface of the electrode. This resulted in (i) increased sensitivity and (ii) a flatter sigmoid — because the fluid was drained, it took less force to achieve a given impedance level. The two curves converged during contact of the textured silicone to the core.

### *3.1.2. Temporal Responses*

All of the responses illustrated in Figs 4 and 5 were actually collected in both directions of loading and unloading, but only rising forces are illustrated. Generally, there was little or no hysteresis over most of the operating range. Figure 6 illustrates the worst case hysteresis, which was seen only at the higher force levels. The time between data points was about 2 s, so the rates of loading and unloading were unphysiologically slow.

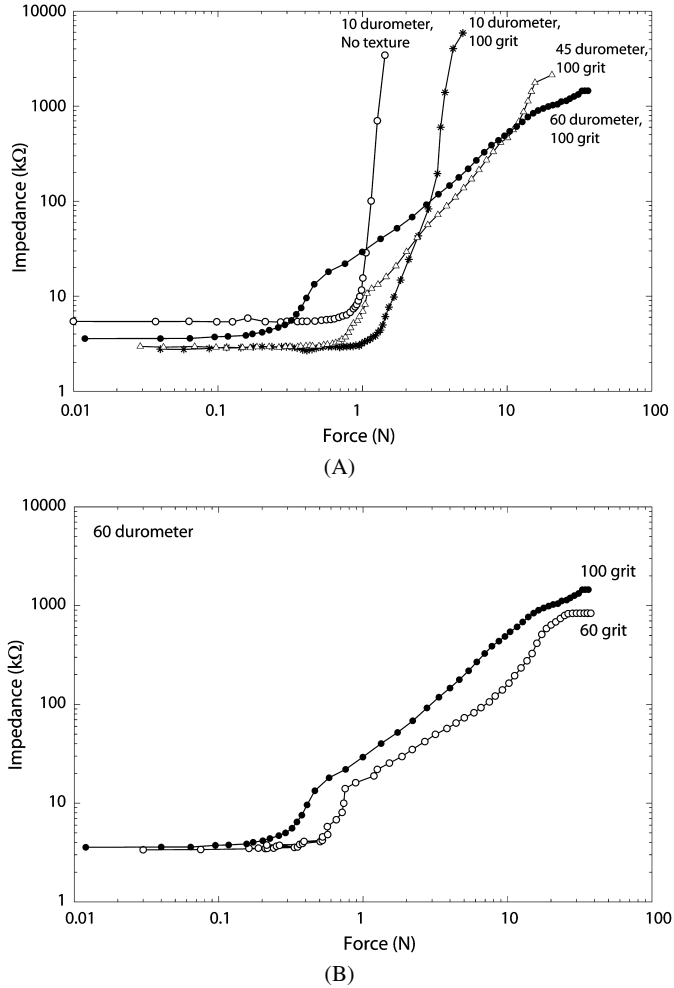


**Figure 5.** (A) Response of sensor to texture stiffness. (B) Response to texture depth (grit size). (C) Response to fluid volume. Panels (A)–(C) show response to the 20-mm probe.

To estimate the true frequency response of the sensors, we applied a vertically oscillating flat probe to the fingertip while recording the vertical force and the envelope of the sinusoidal $V_{\text{out}}$ (Fig. 7). The temporal details of the mechanical input were well represented over the range of frequencies and loads tested informally (approximately 5–15 Hz at 3–5 N in Fig. 7A and 45 Hz at 10–15 N in Fig. 7B).

*3.1.3. Deflection Applied Above and Around the Electrode*

The sensor was systematically probed in a $4 \times 5$ grid; impedance measurements about the electrode of interest, located at $(x, y) = (0, 0)$, demonstrate a spatial resolution below 2 mm (Fig. 8). The spatial resolution is, of course, dependent upon contact location. If a deflection is made far away from any electrode, then resolution will diminish.

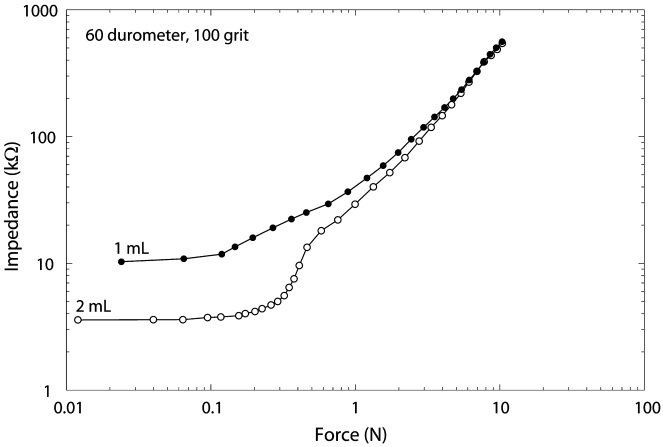


(C)

**Figure 5.** (Continued.)

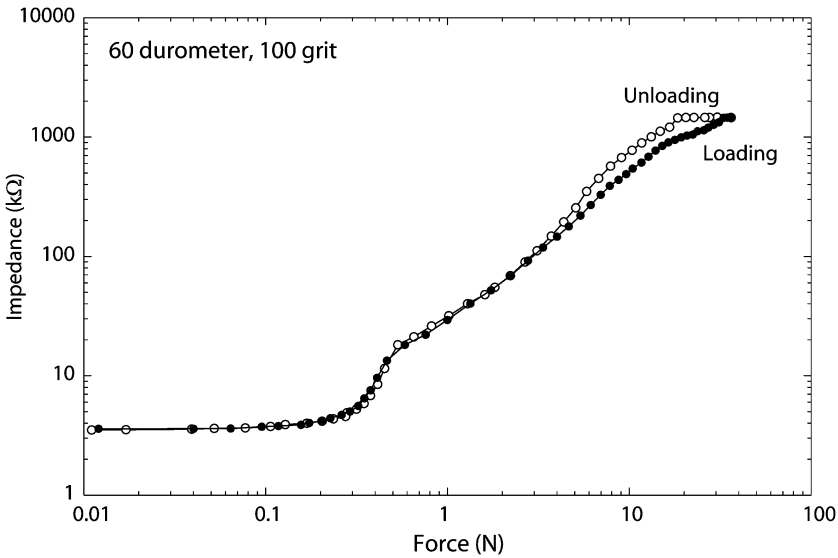


**Figure 6.** Loading/unloading curve (20-mm probe).

## 4. Discussion

The response of a single electrode varied significantly with the radius of curvature and contact surface area of the probe, but generally consisted of three distinct phases of sensing behavior (Fig. 4). During the initial deflection of the skin, the fluid is displaced from between the skin and the core. As the skin is deformed above a given working electrode it constricts the flowpath for ions between the electrode and ground. The impedance rises non-linearly and is related to the overall constriction of the ionic flowpath. In region A, there is relatively little deformation.

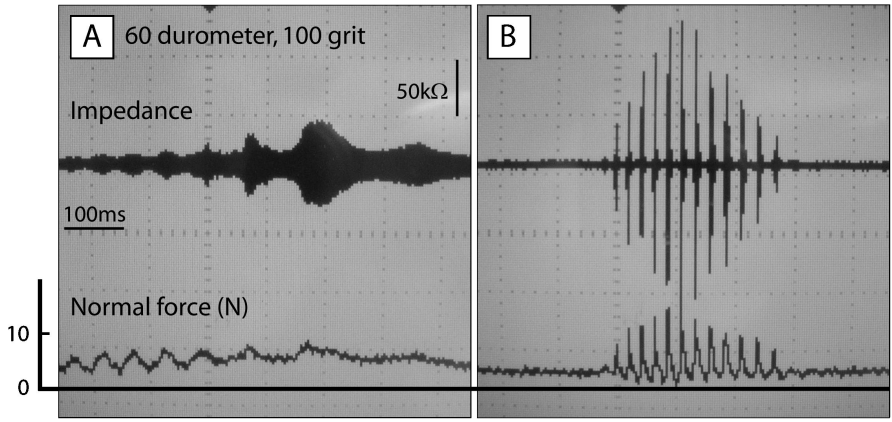


**Figure 7.** (A) 5–15 Hz response of sensor. (B) 45 Hz response of sensor. The force waveform is unidirectional. The impedance waveform is bidirectional because it is capturing the envelope of a sinusoidal waveform.

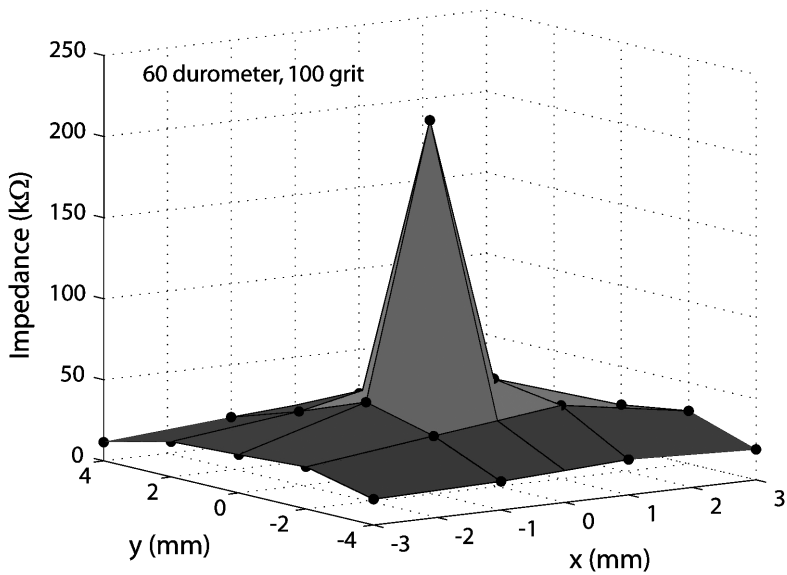


**Figure 8.** Impedance as a function of center of pressure with respect to the location of a working electrode at $(x, y) = (0, 0)$ for 4.5 mm vertical deflections with a 2-mm diameter probe.

In region B, the skin approaches the electrode and begins to contact it, cutting off the fluid access to the electrode and increasing the resistive component of the impedance. In region C, the textured skin has contacted the surface of the electrode and as force increases, the fluid channels through the grooves of the textured surface are gradually compressed (see Fig. 9).

More force is required to compress the channels in the stiffer, high-durometer rubber. This increases the dynamic range of forces before the channels are com-

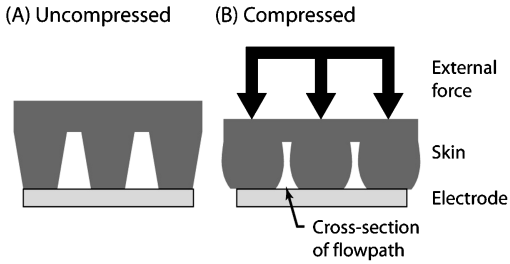


**Figure 9.** (A) The textured rubber is shown in an uncompressed state. (B) An applied force compresses the textured rubber and narrows the flowpath of the fluid to the electrode surface. The impedance measured in condition '(A)' will be lower than that in condition '(B)'.

pletely closed and the measured impedance saturates (Fig. 5A). As the grit size of the texturing is made rougher, this provides deeper channels that require more force to compress (Fig. 5B), also extending the force range. However, if the size of the irregular texturing is made too large in contrast to the size of the electrode, the sensor's behavior will become dependent upon random interactions between the texture features and the electrode surface.

The shape of the remaining conductive path also depends on the shape of the probe. With the 20-mm probe (similar in curvature to the sensor core), there was a gradual rise in impedance and force (region $A_{20}$) for the first 0.2 N of force until the skin contacted the electrode. Then the impedance and force rose rapidly (region $B_{20}$) as the textured inner surface of the skin began to seal to the electrode. Once full contact was made (region $C_{20(1)}$) the sensor exhibited a more linear response until response saturated as maximal occlusion was reached in region $C_{20(2)}$. With the 2-mm probe, the gradual rise in impedance took longer ($A_2$) because the small probe deformed the inner contour of the skin, preventing even contact over the entire electrode surface until it reached a larger deflection ($B_2$). For a small probe similar in size to the diameter of the electrode itself, even a slightly off-center position would affect the transition from region A to B, which would account for the apparent rightward shift of curve region $B_2$ *versus* $B_{20}$ in Fig. 4A. With the flat probe, the impedance did not increase rapidly until force reached 7 N because the force was distributed over a large surface of skin ($A_f$). The flat probe pushed the fluid downward as well as outward, causing a change in the shape of the volumetric flow path, but less change in the impedance than the 20-mm probe. Eventually, the skin contacted the core, producing a steeper increase in both impedance and force ($B_f$) and eventual saturation ($C_f$).

It would appear that there is an ambiguity between impedance and deflection (or force) and the shape of the contacting object. If the shape of the object is not known *a priori*, how is one to determine deflection or force from impedance? This problem is solved through active exploration of the object to obtain other features such as object shape — which is exactly what the human haptic system does. The amount and timing of the deflection is caused by and known to the operator exploring the

object. Thus, the shape can be extracted from the time course of the impedance measured and comparison of the sensor response against the expected values based on *a priori* experience and expectation, as discussed later.

Figure 5A–B describes how modulating the stiffness and depth (grit size) of the texturing affected the force-impedance relationship. Depending upon the force range desired, the internal texturing could be designed accordingly. Figure 5C demonstrates the effect of lower fluid volume and hydrostatic pressure. This resulted in increased sensitivity — the 1-ml curve had a larger impedance initially (as expected from the thinner fluid path), but a more gradual increase over the low range of applied forces. Other factors that would influence this include thickness and compliance of the skin and hydrostatic pressure of the fluid, which remain to be examined systematically.

Figure 6 shows that above 3 N and for unphysiologically slowly changing forces (more than 2 between measurement points) there was noticeable hysteresis. We speculated that the divergence at high force levels may have been caused by static friction between the textured silicone and the lightly abraded surfaces of the electrode contacts and acrylic core, in which case it might be expected to be highly dependent on rate of loading and unloading. This was confirmed by the fast temporal responses to a vibrating flat surface (Fig. 7). We have yet to undertake systematic dynamic testing, but gross hysteresis and drift are not expected in our sensor because the silicone elastomer is a spring-like material that does not exhibit creep and the fluid has low viscosity.

The spatial resolution displayed in Fig. 8 presumably depends on several mechanical factors. These include the dimensions of the probe (2 mm diameter), the electrode (2.3 mm diameter) and the skin (around 4 mm thickness), whose interrelationships remain to be determined systematically.

### *4.1. Feature Extraction*

The positioning of the electrodes with respect to the contours of the core and overlying fluid and skin causes distinct patterns of change in impedance as the sensor contacts objects and surfaces with various force vectors. For example, those electrodes located near the nailbed will detect large increases in impedance when shear forces are directed away from them, pulling the skin close to these electrodes. The following sections summarize phenomena whose characteristic features can be detected by the sensor, in principle.

#### *4.1.1. Contact Force Magnitude*

As the total force increases on the central area of the sensor, the thickness of the fluid layer overlying the electrodes in the compressed region decreases, causing the impedance measurements from the electrodes in that region to increase. The contributions of all such impedance increases are related to the total force of contact.

*4.1.2. Contact Force Direction*

In most object manipulation tasks, the force vector imposed by the contacted object is not perfectly normal to the sensor surface. In biological skin, shear force components change the stress and strain distributions within the fingertip that are sensed by receptors located within dermal and subdermal tissues, but also by the distribution of pressure around the perimeter of the finger pad, particularly where the skin is anchored by the nailbed [29]. This deviation of the force vector from normal is generally associated with a tendency of the grasped object to slip or rotate [29–34]. In our tactile sensing fingertip, shear forces will cause the skin to slide and pull tight over electrodes located where the skin meets the fingernail. As a result, these electrodes will detect large increases in impedance when shear forces are directed away from them.

*4.1.3. Location of Force Centroid*

The impedance increases associated with the contact force measurement previously described can be related to electrode location to estimate the location of the center of force on the skin surface.

*4.1.4. Object Shape*

The relationship between impedance measured at a single electrode and the force applied to an object depends on the shape of the object (Fig. 4), and also on the location of the object with respect to that electrode (Fig. 8) and the radius of curvature of the rigid core on which the electrode is mounted. The impedances measured across an array of such electrodes can, in principle, be used to interpret object shape. For example, a small or narrow object will produce a local deformation of the skin that will cause large changes of impedance for only one or a few electrodes close to the point of contact. A sharp edge will cause an abrupt boundary between electrodes with high impedance and those with low impedance as a result of displacement of fluid and bulging of the skin. The optimal relationships among the curvature of the core, the number and spacing of electrodes, and the thickness and inflation of the skin remain to be determined. Features that are larger than the array will require additional haptic exploration to identify them.

*4.1.5. Object hardness/softness*

As previously stated, the sensor can detect mechanical transients associated with making contact with an object. If the sensor is affixed to a mechatronic finger moving at a known velocity, the rate of deformation increase can be used to indicate the level of hardness or softness of a contacted object. A hard object will cause a rapid increase in deformation (and voltage response) for a given finger velocity when compared to a soft object.

*4.1.6. Contact transients and vibration*

The impedance of the electrodes in the biomimetic fingertip will undergo only very small changes when lightly loaded, but it may be possible to detect such changes by means of their synchronous phasing across the entire array of electrodes [32].

Signal-averaging techniques can be applied to enhance the detection of the correlated component of weak and noisy signals from an array of sensors. Direct measurement of hydrostatic pressure may be preferable, however (see Section 4.3).

### 4.2. Further Feature Characterization

We have demonstrated basic characterization of the sensor with respect to force, deflection and impedance. More thorough testing is required, including thermal response, destructive analysis, etc. Some contact features such as force centroids could be extracted analytically using a reasonable mathematical model. In our array of tactile sensors, force magnitude and point of application interact with each other. For example, a force vector applied close to the nailbed will create a different amount of net impedance change than if the same force vector were applied to the fingertip. Thus, impedance cannot be used as a measure of the applied force unless one accounts for the point of application.

Our sensor array has properties similar to the biological fingertip, however, so it will likely require non-analytical signal processing methods similar to those employed by the biological nervous system. The characterization experiments described above will produce a rich dataset consisting of pairs of input vectors (describing the force vector and its point of application) and output vectors (voltages related to impedances of the electrode array). These will be used to train neural networks for various tasks. This approach can be use to determine the discriminability of various input conditions or, conversely, to determine the ability to generalize a single parameter such as magnitude of forces applied to different portions of the finger tip. For extracting force magnitude and point of application, we will use a multi-layer perceptron and a radial-basis neural network because they are capable of approximating any given non-linear relation when a sufficient number of neurons are provided in the hidden layer [35–37]. Two-point discrimination is also possible, but will depend critically on the thickness and viscoelastic properties of the skin.

### 4.3. Enhancements

In addition to the primary array of electrodes and electrolytic fluid, the sensor can easily be fitted with enhancements and auxiliary systems to provide further sensory information. To enhance vibration sensing, dermal ridges (i.e., fingerprints) can be molded onto the exterior of the elastomer. Human ridges, typically 0.1 mm tall and 0.3–0.5 mm wide, aid in sensing of rough surfaces [38]. Mukaibo *et al.* showed successful application of this principle in their tactile sensor that included a solid distal phalanx coated in a silicone elastomer [39]. They converted texture into vibrations during the stick–slip phenomena as the ridges were run over an object's surface. Biologically, these vibrations are detected by Meissner corpuscles below the epidermal ridges. The frequency of the vibration is:

$$f = \frac{v}{\lambda}, \tag{1}$$

where $f$ is the frequency, $v$ is the finger velocity and $\lambda$ is the peak-to-peak distance between ridges. Such small amplitude vibrations will produce coherent signals in the various contact impedances, but their amplitudes will be small and may be difficult to detect. Alternatively hydrostatic fluid pressure could be sensed by incorporating a hydraulic pressure sensor, doubly serving as a plug, on the proximal end of the fill-tube.

Thermal sensing is also desirable as a part of haptics and could be incorporated in several ways. Saline solutions tend to increase their volume conductivity at higher temperatures (the reverse of solid-state resistors). With our saline electrolytic fluid, we may need to incorporate a thermistor on the surface of the core to adjust the calibration of the impedance sensing. Alternatively, the resting distribution of electrode impedances will reflect ambient temperature. Conventional thermistors mounted on the core will tend to respond slowly to contact with hot or cold objects because the heat capacity of the surrounding fluid and skin will reduce their sensitivity to external objects. We may need to mount a thermistor on the skin itself, a problem that must be solved for any gripping surface that includes a viscoelastic pad to help stabilize contact with objects. For haptic characterization of the material properties of objects, humans actually use heat flow from body temperature. For example, a metallic object will conduct heat away faster than a wooden object. Thus, a heated thermistor may be necessary.

We are currently incorporating multiplexing and conditioning circuitry into the fingertip itself to minimize the number of wires that exit the sensor and the stray capacitance among them. We are developing a flex circuit that will include such circuitry plus the other sensors (thermistor, fluid pressure) and the electrode contacts themselves to simplify fabrication of the whole array. As a result of the relatively low data rates, all values can be transmitted on a serial bus requiring only three or four wires for power and data.

The aqueous solution used to fill the fingertip has the disadvantage of diffusing slowly through the silicone elastomer used for the skin. This problem will need to be addressed either by incorporating a lower permeability layer in the skin covering or a less diffusible solvent for the low conductivity fluid.

## 5. Use of the Tactile Information

Stabilizing grip is an important function whose requirements and natural strategies are becoming better understood. In a series of papers by Roland Johansson and colleagues, it has been shown that grip stability is affected by an object's size, shape, mass and weight distribution, and by the coefficient of friction between the fingertips and surface of the object [34, 40–42]. They have also shown that the central nervous system typically adjusts the grip force so that the friction force developed between the fingertips and the object surface has only a small margin over the external forces that would otherwise cause the object to slip [27, 43]. This strategy is energetically efficient and suitable for manipulating delicate objects that might

be crushed, but it demands continuous tactile sensing and adjustment of grip forces according to the perceived properties of the gripped object.

Each finger's grip force is adjusted independently based on the sensory information from that finger only, and on the local conditions in terms of weight distribution and friction. At least some of this adjustment occurs so rapidly, as quickly as within 40–60 ms [27], that it appears to be mediated reflexively in the spinal cord rather than *via* the brain. This is important for prosthetic limbs because it suggests that tactile information can serve a useful function even if communication channels to provide conscious perception of touch to the operator remain non-existent or primitive, as they are now. Algorithms for the automatic adjustment of grip using biomimetic strategies are likely to be valuable also in telerobotic and purely robotic manipulanda.

We plan to integrate our tactile sensors into the fingertips of a Sarcos dexterous arm robot and train neural network-based controllers to produce patterns of grip force adjustment that mimic those described in psychophysical experiments on human subjects. Fortunately, there is now a rich database describing grip forces and their adjustment in human subjects coping with both predictable and unpredictable pulling loads [27, 42–44]. One strategy for the controller divides the problem into two levels — one trained to extract information about force intensity and distribution, and a higher-level block trained to adjust grip forces based on the extracted sensory information. Another strategy would be to train the robotic hand to behave like a human hand using the raw data from the sensor array as the input layer to the neural network, similar to that of Tada and Hosoda [45].

Realistic grip control will require higher-level control strategies above and beyond reflexive adjustments, perhaps better embodied by discontinuous state machines than by continuous neural networks. Humans can modulate their grip adjustment reflexes to provide a variable margin of safety or to allow voluntary release of objects. Confronted with a novel object, subjects adopt exploratory strategies, slowly decreasing grip force until subtle changes in the distribution of forces in the skin signal incipient slip. They also utilize iterative haptic exploration strategies in which sensory information returned from one exploratory movement of the hand is used to devise the next exploratory movement. These strategies to extract information from tactile sensors are developed over an extended period of skill acquisition. Substantive changes in this tactile information (e.g., as a consequence of injuries to the fingers or their peripheral nerves) require lengthy therapeutic retraining to achieve functional rehabilitation.

## 6. Conclusions

The biomimetic fingertip presented in this work will not by itself solve any of the above problems of object manipulation and identification. It does, however, provide a mechanically robust and informatically rich set of sensors that bears some resemblance to biological tactile sensors. Preliminary tests suggest a wide dynamic

range, distinct phases of sensing at low, medium and high loads, minimal hysteresis, and sensitivity to nearby skin deformations. The robust core protects the sensitive electrical connections and the simple design enables quick repair of the elastomeric skin, as needed. The non-viscoelastic components ensure minimal hysteresis, making possible the development of feedback controllers with short latencies similar to those of humans. Most of the tools and tasks of an industrial world were designed by humans to be performed by human hands in unstructured environments. This motivates the strategy of biomimetic design for prosthetic hands and robotic manipulanda intended to function in this world.

*Acknowledgements*

The authors are grateful to the National Academies Keck Futures Initiative and the Alfred E. Mann Institute for Biomedical Engineering at the University of Southern California for assistance with this project. The authors also thank Crystal Dizol for the CAD design of the distal phalanx, Ray Peck for fabrication and guidance Djordje Popovic for assistance with the electronics and neural network approach, and Nava Davuluri, Juhi Patel and Jesus Robles for their help with the characterization experiments.

## References

1. B. B. Edin, L. Beccai, L. Ascari, S. Roccella, J. J. Cabibihan and M. C. Carrozza, A bio-inspired approach for the design and characterization of a tactile sensory system for a cybernetic prosthetic hand, in: *Proc. IEEE Int. Conf. on Robotics and Automation*, Orlando, FL, pp. 1354–1358 (2006).
2. J. Butterfaß, M. Grebenstein, H. Lui and G. Hirzinger, DLR-Hand II: next generation of a dexterous robot hand, in: *Proc. IEEE Int. Conf. on Robotics and Automation*, Seoul, pp. 109–114 (2001).
3. A. Mishkin, Y. Lee, D. Korth and T. LeBlanc, Human–robotic missions to the Moon and Mars: operations design implications, in: *Proc. IEEE Aerospace Conf.*, Big Sky, MT, pp. 1–10 (2007).
4. S. Sokhanvar, M. Packirisamy and J. Dargahi, A multifunctional PVDF-based tactile sensor for minimally invasive surgery, *Smart Mater. Struct.* **16**, 989–998 (2007).
5. A. P. Miller, W. J. Peine, J. S. Son and Z. T. Hammoud, Tactile imaging system for localizing lung nodules during video assisted thoracoscopic surgery, in: *Proc. IEEE Int. Conf. on Robotics and Automation*, Rome, pp. 10–14 (2007).
6. R. D. Howe, W. J. Peine, D. A. Kantarinis and J. S. Son, Remote palpation technology, *IEEE Eng. Med. Biol. Mag.* **14**, 318–323 (1995).
7. J. Tegin and J. Wikander, Tactile sensing in intelligent robotic manipulation — a review, *Ind. Robot* **32**, 64–70 (2005).
8. M. H. Lee and H. R. Nichols, Tactile sensing for mechatronics — a state of the art survey, *Mechatronics* **9**, 1–31 (1999).
9. L. Beccai, S. Roccella, A. Arena, F. Valvoa, P. Valdastria, A. Menciassia, M. C. Carrozza and P. Dario, Design and fabrication of a hybrid silicon three-axial force sensor for biomechanical applications, *Sensors Actuators A* **120**, 370–382 (2005).
10. T. Mei, W. J. Li, Y. Ge, Y. Chen, L. Ni and M. H. Chan, An integrated MEMS three-dimensional tactile sensor with large force range, *Sensors Actuators A* **80**, 155–162 (2000).

11. D. J. Beebe, A. S. Hsieh, R. G. Radwin and D. D. Denton, A silicon force sensor for robotics and medicine, *Sensors Actuators A* **50**, 55–65 (1995).
12. D. Bloor, K. Donnely, P. J. Hands, P. Laughlin and D. Lussey, A metal-polymer composite with unusual properties, *J. Phys. D Appl. Phys.* **38**, 2851–2860 (2005).
13. G. Vasarhelyi, M. Adam, E. Vazsonyi, I. Barsony and C. Ducso, Effects of the elastic cover on tactile sensor arrays, *Sensors Actuators A* **132**, 245–251 (2006).
14. V. Shamanna, S. Das, Z. Çelik-Butler, D. P. Butler and K. L. Lawrence, Micromachined integrated pressure–thermal sensors on flexible substrates, *J. Micromech. Microeng.* **16**, 1984–1992 (2006).
15. M. Lowe, A. King, E. Lovett and T. Papakostas, Flexible tactile sensor technology: bringing haptics to life, *Sensor Rev.* **24**, 33–36 (2004).
16. M. Helsel, J. N. Zemel and V. Dominko, An impedance tomographic tactile sensor, *Sensors Actuators* **14**, 93–98 (1988).
17. R. A. Russell, A tactile sensor skin for measuring surface contours, in: *Proc. IEEE Region 10 Int. Conf. on Technology Enabling Tomorrow: Computers, Communications and Automation towards the 21st Century*, Melbourne, pp. 262–266 (1992).
18. R. A. Russell and S. Parkinson, Sensing surface shape by touch, in: *Proc. IEEE Int. Conf. on Robotics and Automation*, Atlanta, GA, vol. 1, pp. 423–428 (1993).
19. G. Kenaly and M. Cutkosky, Electrorheological fluid-based robotic fingers with tactile sensing, in: *Proc. IEEE Int. Conf. on Robotics and Automation*, Scottsdale, AZ, vol. 1, 132–136 (1989).
20. R. Voyles, G. Fedder and P. Khosla, Design of a modular tactile sensor and actuator based on an electrorheological gel, in: *Proc. IEEE Int. Conf. on Robotics and Automation*, vol. 1, 132–136 (1989).
21. R. S. Johansson and G. E. Loeb, Biomimetic tactile sensor, *US provisional patent 60/786,607* (2006).
22. N. Wettels, D. Popovic, V. J. Santos, R. S. Johansson and G. E. Loeb, Biomimetic tactile sensor for control of grip, in: *Proc. Int. Conf. on Rehabilitation Robotics*, Noordwijk, pp. 923–932 (2007).
23. Y. K. Lee, B. S. Lim and C. W. Kim, Mechanical properties of calcium phosphate based dental filling and regeneration materials, *J. Oral Rehabil.* **30**, 418–425 (2003).
24. D. Merrill, M. Bikson and J. Jeffreys, Electrical stimulation of excitable tissue: design of efficacious and safe protocols, *J. Neurosci. Methods* **141**, 171–198 (2005).
25. A. Dalmia, C. C. Liu and R. F. Savinell, Electrochemical behavior of gold electrodes modified with self-assembled monolayers with an acidic end group for selective detection of dopamine, *J. Electrochemistry* **430**, 205–214 (1997).
26. B. Piela and P. Wrona, Capacitance of the gold electrode in 0.5 M sulfuric acid solution: AC impedance studies, *J. Electrochem.* **388**, 69–79 (1994).
27. R. S. Johansson, R. Riso, C. Hager and L. Backstrom, Somatosensory control of precision grip during unpredictable pulling loads. I. Changes in load force amplitude, *Exp. Brain Res.* **89**, 181–191 (1992).
28. G. E. Loeb and W. B. Marks, Optimal control principles for sensory transducers, in: *The Muscle Spindle*, I. A. Boyd and M. H. Gladden (Eds), pp. 409–415. Macmillan, London (1985).
29. I. Birznieks, P. Jenmalm, A. W. Goodwin and R. S. Johansson, Encoding of direction of fingertip forces by human tactile afferents, *J. Neurosci.* **21**, 8222–8237 (2001).
30. J. R. Flanagan, M. K. O. Burstedt and R. S. Johansson, Control of fingertip forces in multi-digit manipulation, *J. Neurophys.* **81**, 1706–1717 (1999).
31. R. S. Johansson and G. Westling, Roles of glabrous skin receptors and sensorimotor memory in automatic control of precision grip when lifting rougher or more slippery objects, *Exp. Brain Res.* **56**, 550–564 (1984).

32. G. Westling and R. S. Johansson, Responses in glabrous skin mechanoreceptors during precision grip in humans, *Exp. Brain Res.* **66**, 128–140 (1987).
33. R. S. Johansson and G. Westling, Signals in tactile afferents from the fingers eliciting adaptive motor responses during precision grip, *Exp. Brain Res.* **66**, 141–154 (1987).
34. R. S. Johansson and J. R. Flanagan, Tactile sensory control of object manipulation in human, in: *Handbook of the Senses, Vol. 5: Somatosensation*, J. Kaas and E. Gardner (Eds), pp. 67–86, Elsevier, Amsterdam (2007).
35. K. Hornik, M. Stinchcombe and H. White, Multilayer feed forward networks are universal approximators, *Neural Networks* **2**, 359–366 (1989).
36. J. Park and I. Sandberg, Approximation and radial-basis-function networks, *Neural Comput.* **5**, 305–316 (1993).
37. M. Caudill and C. Butler, *Understanding Neural Networks: Computer Explorations. Vol. 1. Basic Networks*. MIT Press, Cambridge, MA (1992).
38. D. Yamada, T. Maeno and Y. Yamada, Artificial finger skin having ridges and distributed tactile sensors used for grasp force control, in: *Proc. IEEE/RSJ Int. Conf. on Intelligent Robots and Systems*, Maui, HI, pp. 686–691 (2001).
39. Y. Mukaibo, H. Shirado, M. Konyo and T. Maeno, Development of a texture sensor emulating the tissue structure and perceptual mechanism of human fingers, in: *Proc. IEEE Int. Conf. on Robotics and Automation*, Barcelona, pp. 2576–2581 (2005).
40. R. S. Johansson and G. Westling, Role of glabrous skin receptors and sensorimotor memory in automatic control of precision grip when lifting rougher and more slippery objects, *Exp. Brain Res.* **56**, 550–564 (1984).
41. K. J. Cole and R. S. Johansson, Friction at the digit-object interface scales the sensory-motor transformation for grip responses to pulling loads, *Exp. Brain Res.* **95**, 523–532 (1993).
42. R. S. Johansson, C. Hager and R. Riso, Somatosensory control of precision grip during unpredictable pulling loads. II. Changes in load force rate, *Exp. Brain Res.* **89**, 192–203 (1992).
43. A. Gordon, G. Westling, K. J. Cole and R. S. Johansson, Memory representation underlying motor commands used during manipulation of common and novel objects, *J. Neurophys.* **69**, 1789–1796 (1993).
44. R. S. Johansson and I. Birznieks, First spikes in ensembles of human tactile afferents code complex spatial fingertip events, *Nat. Neurosci.* **7**, 170–177 (2004).
45. Y. Tada and K. Hosoda, Acquisition of multi-modal expression of slip through pick-up experiences, in: *Proc. IEEE/RSJ Int. Conf. on Intelligent Robots and Systems*, Beijing, pp. 5810–5815 (2006).

## About the Authors

**Nicholas Wettels** received the BS degree in Physics with a Minor in Mathematics from Tulane University, New Orleans, LA, in 2000, and the MS degree in Engineering Management from Old Dominion University, Norfolk, VA, in 2005. In 2000, he was commissioned in the US Navy as a submarine officer. After tours aboard the attack submarine *USS Topeka* (SSN-754) and Navy Recruiting District — Los Angeles, he ended his 7 years of active duty to begin his career as a Navy reserve officer and attend graduate school at University of Southern California, Los Angeles, CA. He is currently a biomedical engineering PhD student under Dr Gerald E. Loeb. His research interests include neuroprosthetics, artificial somatosensory feedback and haptic identification of objects. He has received a Best Student Paper Award at the ASME 2nd

Frontiers in Biomedical Devices Conference, Irvine, CA (2007), the Navy GEV Scholarship (2005) and a Tulane University NROTC Scholarship (1997).

**Veronica J. Santos** received the BS degree in Mechanical Engineering with a Music Minor from the University of California at Berkeley, CA, in 1999, and the MS and PhD degrees in Mechanical Engineering with a Biometry Minor from Cornell University, Ithaca, NY in 2004 and 2007, respectively. She is currently a Postdoctoral Research Associate at the A. E. Mann Institute for Biomedical Engineering at the University of Southern California, Los Angeles, CA. From 2000 to 2001, she was a Quality Engineer and Research and Development Engineer at Guidant Corporation in Santa Clara, CA, specializing in life-saving cardiovascular technology. Her research interests include hand biomechanics, neural control of movement, robotics, stochastic modeling, and clinical applications of biomechanical modeling for rehabilitation technology and surgical procedures. She has received the Young Investigator Poster Presentation Award from the International Society of Biomechanics (2005), an Exceptional Teaching Assistant Award from the Sibley School of Mechanical and Aerospace Engineering at Cornell University (2005), and a National Science Foundation Graduate Research Fellowship (2001).

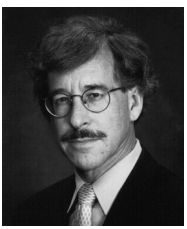

**Gerald Loeb** received a BA and a MD from Johns Hopkins University, in 1969 and 1972, and did 1 year of surgical residency at the University of Arizona before joining the Laboratory of Neural Control at the National Institutes of Health (1973–1988). He was Professor of Physiology and Biomedical Engineering at Queen's University in Kingston, Canada (1988–1999) and is now Professor of Biomedical Engineering and Neurology and Director of the Medical Device Development Facility of the A. E. Mann Institute for Biomedical Engineering at the University of Southern California. He was one of the original developers of the cochlear implant to restore hearing to the deaf and was Chief Scientist for Advanced Bionics Corp. (1994–1999), manufacturers of the Clarion® cochlear implant. He is a Fellow of the American Institute of Medical and Biological Engineers, holder of 43 issued US patents and author of over 200 scientific papers. Most of his current research is directed toward neural prosthetics to reanimate paralyzed muscles and limbs using a new technology that he and his collaborators developed called BIONs®. This work is supported by an NIH Bioengineering Research Partnership and is one of the testbeds in the NSF Engineering Research Center on Biomimetic MicroElectronic Systems, for which he is Deputy Director. These clinical applications build on his long-standing basic research into the properties and natural activities of muscles, motoneurons, proprioceptors and spinal reflexes.

**Roland S. Johansson** received the Bachelor of Medicine degree in 1974, Doctor of Medicine in 1978 and was qualified as Docent in Physiology in 1981, all at the University of Umeå, Umeå, Sweden. He has been a Professor of Physiology in the Department of Integrative Medical Biology (Physiology Section), Umeå University, since 1988. His previous positions include Chair at the Department of Physiology 1988–1996, and Associate Professor ('docent' appointment) in Physiology, 1983–1988, all at the University of Umeå. He was also a Visiting Scientist at the Department of Anesthesiology, Yale University, School of Medicine, New Haven, CT, 1981–1982, and Assistant Professor in Physiology, University of Umeå, 1979–1981. He is the Primary Investigator for the Dexterous Manipulation Laboratory. The overall research goal is to unravel the neural sensorimotor mechanisms that endow humans with their extraordinary ability to manipulate physical objects with their hands. Specifically, we want to capture the relevant schemes of the automatically operating task-dependent interactions between various sensory and motor mechanisms used in dexterous manipulation. These include memory mechanisms that establish motor output parameters and sensorimotor transformations.